International Journal of Coal Geology 225 (2020) 103479

Contents lists available at ScienceDirect

International Journal of Coal Geology

journal homepage: www.elsevier.com/locate/coal

A two-stage step-wise framework for fast optimization of well placement in coalbed methane reservoirs

Jiyuan Zhang[a,b,*], Qihong Feng[a,b,*], Xianmin Zhang[a,b], Jia Bai[c], C. Özgen Karacan[d], Ya Wang[e], Derek Elsworth[f]

[a] Key Laboratory of Unconventional Oil & Gas Development, China University of Petroleum (East China), Ministry of Education, Qingdao 266580, PR China
[b] School of Petroleum Engineering, China University of Petroleum (East China), Qingdao 266580, Shandong, PR China
[c] Xinzhou Branch Company, PetroChina Coalbed Methane Company Ltd., Xinzhou 036600, Shanxi, PR China
[d] US Geological Survey, Eastern Energy Resources Science Center, Reston, VA 20192, USA
[e] Engineering and Technology Research Institute, PetroChina Coalbed Methane Company Ltd., Xi'an 710082, Shaanxi, PR China
[f] Department of Energy and Mineral Engineering, G3 Center and Energy Institute, The Pennsylvania State University, University Park, PA 16801, USA

ARTICLE INFO

Keywords:
Coalbed methane
Well placement optimization
Step-wise procedure
Well pattern description
Quality map

ABSTRACT

Coalbed methane (CBM) has emerged as a clean energy resource in the global energy mix, especially in countries such as Australia, China, India and the USA. The economical and successful development of CBM requires a thorough evaluation and optimization of well placement prior to field-scale exploitation. This paper presents a two-stage, step-wise optimization framework to obtain the optimal placement of wells for large-scale development of CBM reservoirs. In the first stage, an optimal uniform well pattern is obtained by optimizing well pattern description parameters with the particle swarm optimization (PSO) algorithm. Subsequently, the location and status (active/inactive) of each well are perturbed and optimized within the patterns through the integration of the generalized pattern search (GPS) algorithm and a quality map (QM) representing the production potential. This framework was tested in a synthetic anthracite CBM reservoir in the Qinshui basin (with high gas content and low permeability) and a real field high volatile bituminous reservoir in the Illinois basin (with low gas content and high permeability). The results show that: (i) significant variations in the net present value (NPV) exist with respect to different uniform well patterns (even for cases where the total number of wells are identical), the optima of which can be efficiently determined by the PSO within 100 numerical simulation runs; (ii) the optimization of well perturbations by the GPS results in a more noticeable improvement in NPVs for the synthetic (12.3%) than for the real field model (4.6%); (iii) for the low permeable synthetic model with narrow optimal well spacings (320 m × 200 m), the contribution of the optimization of well perturbation to the NPV increment is heavily dependent on the uniform well placement solution; (iv) for the high permeable real field model with large optimal well spacings (1300 m × 1300 m), the initial uniform well placement has a very minor effect on the subsequent well perturbation solutions in terms of NPV; (v) the proposed framework significantly outperforms the conventional well-by-well concatenation procedure in terms of computational efficiency, robustness and optimal criteria set for production potential.

1. Introduction

Development of coalbed methane (CBM) as an energy resource offers subsidiary benefits, such as improving underground coal mining safety and reducing methane emission to the atmosphere (Karacan et al., 2011). However, CBM drainage, especially from low-permeability coal seams, usually has low recovery efficiency. Therefore, special well completions and production mechanisms are needed to achieve commercial gas rates (Ozkan and Clarkson, 2012). Although enhancement techniques, such as the multi-lateral horizontal drillings (Keim et al., 2011) and CO_2 enhanced CBM (CO_2-ECBM) (Ross et al., 2009; Zhou et al., 2013) can be utilized to increase the CBM production, further field tests are needed to validate their technical and economic feasibility (Moore, 2012). For example, multi-lateral horizontal wells may have the high risk of being collapsed that significantly reduces gas production and hence the economics (Keim et al., 2011; Ren et al., 2014). As such, the vertical wells stimulated with hydraulic fractures (Badri et al., 2000) still act as a primary and most reliable means for

* Corresponding authors.
E-mail addresses: zhjy221@126.com (J. Zhang), fengqihong@126.com (Q. Feng).

https://doi.org/10.1016/j.coal.2020.103479
Received 16 September 2019; Received in revised form 7 April 2020; Accepted 7 April 2020
Available online 24 April 2020
0166-5162/

large-scale field development of CBM resources especially for low-permeability coal seams (Palmer, 2010).

Previous studies (Feng et al., 2012; Salmachi et al., 2013, 2014) suggest that the economics of a CBM development project using vertical wells is highly dependent on the well locations. Numerous investigations document the determination of optimal well placement in CBM reservoirs based on analytical models or numerical simulations. Clarkson and McGovern (2005) developed an approach to optimize CBM exploration and development strategies through the integration of the Monte Carlo simulation, reservoir simulation and economics. Xu et al. (2013) derived an analytical mathematical model based on the concept of "balanced depressurization" to optimize well pattern and spacing for hydraulically fractured wells in anisotropic CBM reservoirs. Zuber et al. (1990) studied the gas production and economic prospects of various well-spacing and hydraulic-fracture scenarios through numerical simulation and found that permeability and achievable hydraulic-fracture dimensions are the key parameters for the optimization of well spacing. The work by Wicks et al. (1986), Young et al. (1992), Chaianansutcharit et al. (2001), and Bumb and McKee (1984) led to the common conclusion that pressure interference exerts favorable effects on gas production and drilling more wells can enhance the ultimate recovery factor. It should be noted, however, that the drainage efficiency of uniform well patterns—such as five-spot and rectangular patterns may be questionable when applied in CBM reservoirs that exhibit strong heterogeneities (Cai et al., 2011; Liang et al., 2011; Pashin, 2010; Yao et al., 2013). Besides, the consideration of optimal well spacing must be made based on an economic decision (Zulkarnain, 2005).

During the past decade, a number of investigations have been reported on the use of numerical simulation integrated with statistical analysis or intelligent optimization algorithms to determine optimal well placement in underground hydrocarbon reservoirs (Bangerth et al., 2006; Chen et al., 2018, 2019; Forouzanfar and Reynolds, 2014; Humphries and Haynes, 2015; Humphries et al., 2014; Isebor et al., 2014; Jesmani et al., 2016; Wang et al., 2016, 2019; Zhang et al., 2017). Feng et al. (2012) and Salmachi et al. (2013) optimized the location of vertical wells in CBM reservoirs using numerical simulation assisted by the particle swarm optimization (PSO) and genetic algorithm (GA), respectively. Salmachi et al. (2014) combined numerical simulation with detection theory (decision trees) to find the potential optimal locations of infilling wells in the development of a synthetic CBM reservoir. A distinguished advantage of using optimization algorithms is that a broader set of scenarios can be systematically explored in order to find optimal solutions for some given conditions (Bangerth et al., 2006). However, for large-scale multi-well field development, optimization can be particularly challenging due to a large number of variables and an extensive search space (Zhang et al., 2014). An increment in the search dimensions (number of optimization variables) tends to increase the risk of getting trapped in local optima during the optimization process, rather than finding the global optimum. Consequently, it is important to construct an efficient and robust method to deliver a set of nearly optimal solutions (Bangerth et al., 2006). Unfortunately, few efforts have been made to reach such optimal solutions with respect to the development of CBM reservoirs.

This paper presents a step-wise optimization framework for fast determination of the optimal well placement for the large-scale development of CBM resources. The proposed framework was applied in both a synthetic and a real CBM reservoir, whose performance was compared with the conventional well-by-well concatenation method.

2. Methodology

In this study, the optimal placement of wells is obtained by a step-wise procedure consisting of two stages (Fig. 1). In the first stage, the well pattern and spacings are optimized to determine an optimal uniform layout of wells. Once the optimal well pattern and spacings are determined, the location of each well can be identified, which provides the initial solution to the second step. In the second step, the location of each well is perturbed and optimized based on a quality map (QM) that considers the boundary constraint defined by the well spacings in the previous step.

2.1. Uniform well placement and well perturbation

2.1.1. Description of uniform well placement (step 1)

Two typical well patterns, namely rectangular and five-spot patterns are commonly used for primary drainage of CBM (Tang and Li, 2013). For both well patterns, the layout of wells is designed along two orthogonal directions following principal permeabilities, which can also be proxied as parallel to the face and butt cleat directions (which are represented as X- and Y-directions, respectively in Fig. 1). In this study, we use three variables to represent the layout of wells, $\{s_x, s_y, Index\}$, where s_x, s_y specify well spacings along the X- and Y-directions, respectively, and *Index* denotes the well pattern. Each well is assumed to be placed at the center of a grid block, which is a general default setting method in numerical reservoir simulations. It is noted that for a reservoir model consisting of uniform grid blocks, well spacings s_x and s_y should always be a multiple of the grid block dimensional lengths of d_x and d_y, respectively. For a given uniform well pattern description vector of $\{s_x, s_y, Index\}$, the well locations (coordinates in terms of grid block numbers along X- and Y-directions) can be determined as follows.

2.1.1.1. Calculate the maximum number of wells that can be accommodated within the reservoir. Under the assumption that each well is placed at the center of a grid block, the maximum rows of wells that can be placed along the X- ($n_{x,max}$) and Y- ($n_{y,max}$) directions within the reservoir can be identified as:

$$n_{x,max} = floor\left[\frac{d_x\cdot(N_x-1)}{s_x}\right]+1 \tag{1}$$

$$n_{y,max} = floor\left[\frac{d_y\cdot(N_y-1)}{s_y}\right]+1 \tag{2}$$

where N_x and N_y are the number of grid blocks along the X- and Y-directions, respectively; $floor[\bullet]$ denotes the maximum integer that is not higher than the argument "•" in the brackets.

2.1.1.2. Determine the locations of $n_{x,max}\times n_{y,max}$ wells. Once the number of wells is determined, these wells can then be uniformly deployed across the reservoir plane subject to the well pattern description vector.

For a rectangular well pattern, the location (λ, η) of a well in the ith column and jth row, represented with grid block coordinates, can be calculated straightforwardly by considering the well layout and reservoir geometry (see Fig. 2a for details):

$$\lambda = ceil\left\{\frac{0.5[N_x d_x-(n_{x,max}-1)s_x]+s_x(i-1)}{d_x}\right\} \tag{3}$$

$$\eta = ceil\left\{\frac{0.5[N_y d_y-(n_{y,max}-1)s_y]+s_y(j-1)}{d_y}\right\} \tag{4}$$

where $ceil[\bullet]$ denotes the minimum integer that is higher than the argument "•" in the brackets.

For the five-spot well pattern, wells in odd numbered rows are assigned to be placed the same as in the rectangular well pattern and therefore the locations can be determined using Eqs. 3 and 4. Compared with the rectangular well pattern, the five-spot pattern has one less well in the even numbered rows (Fig. 2). Again, combining the well layout and reservoir geometry, one can obtain the coordinate (λ, η) for wells at the even numbered rows, which can be written as (see Fig. 2b for details):

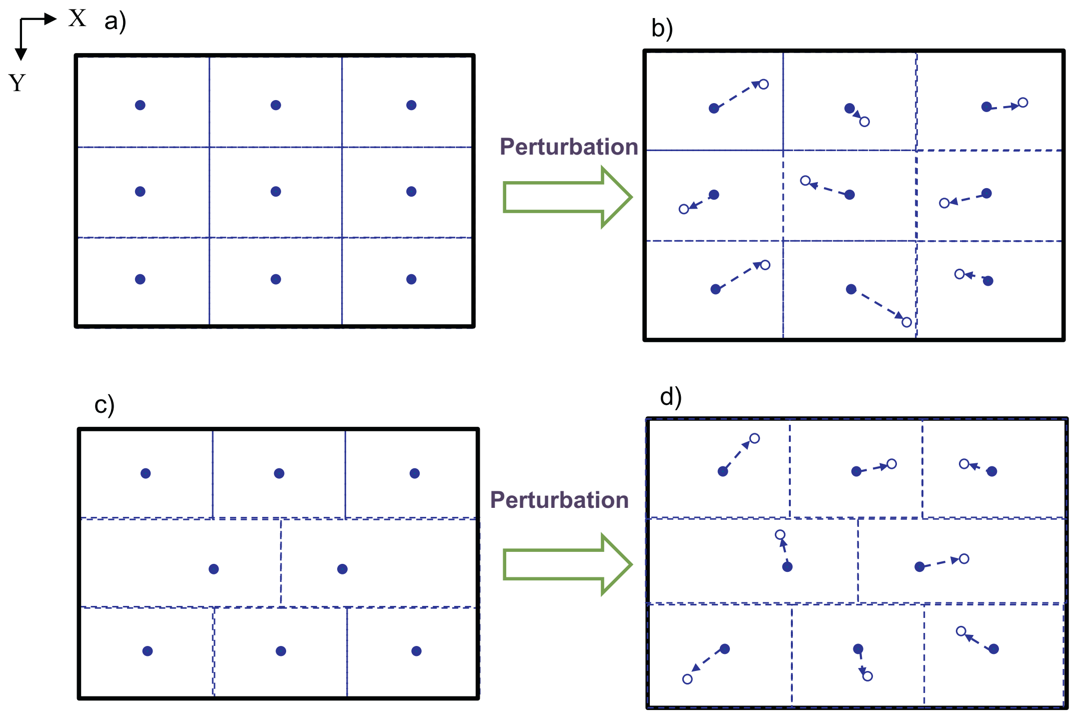

Fig. 1. Uniform rectangular (a) and five-spot (c) well patterns and their corresponding perturbed well locations (b and d). The dashed rectangular block represents the boundary constraining well perturbation. Solid and open circles represent locations of wells before and after perturbation, respectively. Thick solid lines are reservoir boundaries.

$$\lambda = ceil\left\{\frac{0.5[N_x d_x - (n_{x,max} - 2)s_x] + s_x(i-1)}{d_x}\right\} \tag{5}$$

$$\eta = ceil\left\{\frac{0.5[N_y d_y - (n_{y,max} - 1)s_y] + s_y(j-1)}{d_y}\right\} \tag{6}$$

2.1.2. Perturbation of wells (step 2)

For reservoirs exhibiting strong heterogeneity in permeability, it is reasonable to improve the solution further by performing optimization via perturbations of the well locations determined from the regular well pattern. To improve the optimization efficiency, we propose a perturbation procedure that invokes the concept of a QM, which has proven to significantly improve the optimization efficiency of well placement optimization problems (Ding et al., 2014, 2019; Nakajima and Schiozer, 2003).

It is recognized (Feng et al., 2012; Salmachi et al., 2013) that coal seam permeability and gas content are two key factors influencing optimal well placement - wells are more apt to be placed in areas with higher permeability and higher gas content in order to improve the economics. The underlying mechanism behind this conclusion is that higher gas content provides an elevated gas reserve with an increase in mass released once pressure drawdown occurs, while higher permeability ensures a greater flow rate tapping an expanded volume of the reservoir. These two factors improve gas production rates and hence the economics of the operation. As such, it is reasonable to assume by analogy that the grid blocks with higher permeability and higher gas content are potential near-optimal positions for accommodating wells. In this paper, we suggest using an index to rank the production potential of a grid block, which is defined as:

$$IOP_i^j = k_i^j c_i^j h_i^j \tag{7}$$

where k is permeability; c is gas content, h is thickness; the subscript i represents the i^{th} well; and superscript j represents the j^{th} grid block near the i^{th} well. For a specific well, the "grid blocks near" are those within its own control/tributary area ($s_x \times s_y$).

It should be noted that for a multiple well placement problem, all wells being shifted to the grid block with their respective highest IOP_i does not guarantee a global optimum. This is because there is the possibility that wells may be moved to their respective tributary grid blocks that are i) within a narrow distance to other wells or ii) close to boundaries (Fig. 3). To resolve such contradiction, we assign a threshold number of grid blocks with high IOPs for each well as the potential optimal candidates. Each potential candidate has an equal probability to be chosen as the optimal solution, whereas the other grid blocks with lower IOPs will never be selected. In this regard, the perturbation vector can be written as:

$$\boldsymbol{x}' = \left\{\underbrace{\theta_1}_{Well1}, \underbrace{\theta_2}_{Well2}, \ldots, \underbrace{\theta_n}_{Welln}\right\} \tag{8}$$

where θ_i denotes the numbering of a grid block sorted in a descending order of IOP for the i^{th} well. For example, if we assign a number of N grid blocks that are ready to be selected as the candidate perturbed position, $\theta_i = 1$ represents the grid block with the highest IOP while $\theta_i = N$ represents the grid block with the lowest IOP for the i^{th} well. $\theta_i = 0$ represents that the well remains in its original location in the uniform well pattern and no perturbation occurs.

In addition to well position perturbations, the perturbation of well status (inactive or active) can also be optimized in order to further improve the NPV (Onwunalu, 2010) by eliminating redundant wells. This strategy should benefit heterogeneous reservoirs where wells in some local regions are associated with extreme low producibility. In this study, the perturbation of well status can be easily incorporated by extending θ to a negative value. For the i^{th} well, $\theta_i < 0$ represents that this well is inactive, i.e., this well is removed from the reservoir model.

As such, the optimization of well perturbation is transformed to a combinational optimization problem, i.e., we target to optimize the selection of candidate grid block and inactive/active status for each well so that the combination of all the selections for all wells results in an optimal solution.

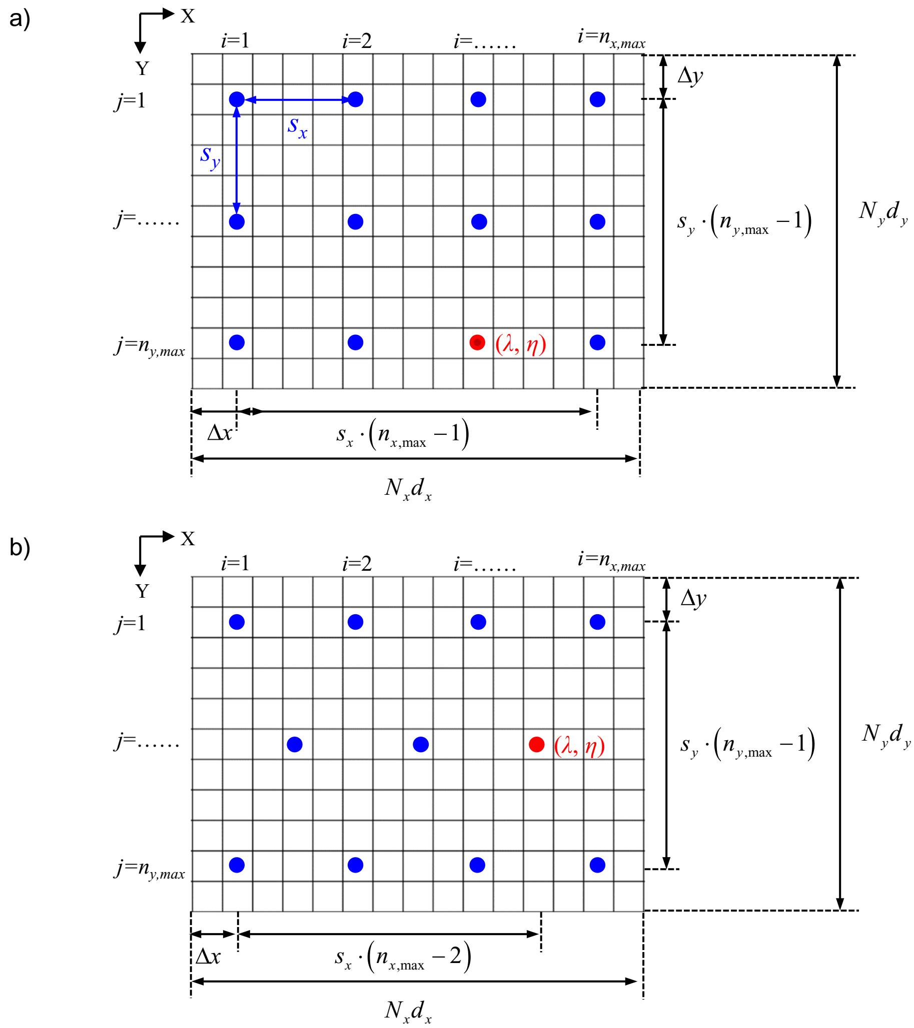

Fig. 2. Illustration of how to calculate uniform well locations for (a) rectangular and (b) five-spot well patterns.

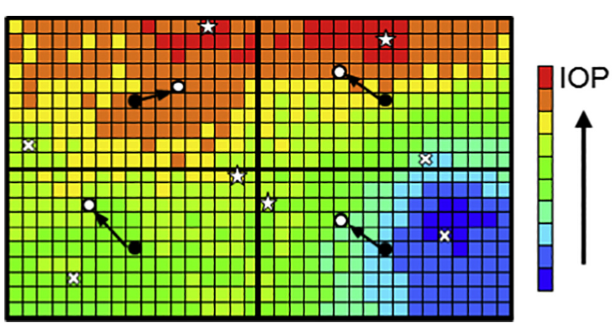

Fig. 3. Illustration of well perturbation with a background of IOP. Solid circle – optimal uniform well placement; open circle – optimal well perturbation; star – grid block with the highest IOP; cross – grid block with the lowest IOP. A grid block on or adjacent to the boundary has the highest IOP for the upper two wells, respectively, which however are not the optimal perturbation solutions because wells on or adjacent to the boundary have significantly less producibility due to their limited controlling area; The grid blocks with the highest IOPs for the respective lower two wells are grouped closely to each other, and neither is the optimal perturbation solution also due to the limited controlling areas of wells.

2.2. Optimization algorithms

To date, numerous optimization algorithms have been applied for solving well placement problems, which generally fall into two categories: gradient-based and derivative-free methods (Bangerth et al., 2006). The solution surface to a well placement problem can be extremely rough and discontinuous gradients may exist. Additionally, gradient-based methods are more likely to be trapped in local optima compared with derivative-free algorithms because well placement problems are usually nonconvex and may contain multiple local optima (Wang et al., 2016). As a comparison, the derivative-free methods do not require the gradient information but only need the objective function value as a guide for their evolution. Such merit makes derivative-free methods more efficient in solving problems such as the optimization of well placement for the development of hydrocarbon reservoirs.

In this paper, two derivative-free algorithms were used for solving the proposed two-stage well placement optimization problem namely particle swarm optimization (PSO) and generalized pattern search (GPS). Numerous studies (e.g., Ding et al., 2019; Wang et al., 2019; Onwunalu and Durlofsky, 2010) have demonstrated the robustness of these two algorithms in solving oilfield optimization problems in terms of convergence speed and accuracy. PSO is a stochastic global search method that is especially suitable for optimization problems without prior knowledge of a near-optimal solution, while GPS is quite efficient when a high-quality initial guess of the optima is available. Onwunalu and Durlofsky (2011) show that well perturbations help improve the economics over a uniform well placement pattern; however, such improvement is less significant than that during the optimization phase for a uniform well pattern. This indicates that the optimization of a uniform well pattern is possibly a global optimization problem whereas optimization of well perturbation is a local one. In this respect, we set the PSO for determining the optimal well pattern and spacings, and the GPS for solving the well perturbation problem. Mathematical details of PSO and GPS algorithms are well described in Torczon (1997), Audet and Dennis Jr. (2002), Kennedy and Eberhardt (1995), and Kaveh (2014), which are therefore not repeated in this paper.

2.3. Objective function

In this study, net present value (NPV) is used as the objective function. NPV is a measure of profitability - that is the present value of cash flows discounted at an average annual discount rate, i_0, in excess of the present value of the investment (Luo et al., 2011). The basic capital costs for a CBM well include outlays for land, permits, drilling, completion, infrastructure (water handling facilities, electric power and electrical cable, gas gathering and transmission facilities, etc.), well maintenance, and water management (ARI, 2002; Bank and Kuuskraa, 2006). For practical consideration, the capital costs are reduced to three parts: well construction, water disposal cost and well operating expense. Construction of wells is assumed to be completed in the first year for all drilling scenarios. The NPV can be calculated as:

$$\mathrm{NPV} = \sum_{t=1}^{T}\left[\frac{Q_g P_g (1-R_t) - Q_w C_w - C_m N_w}{(1+i_0)^t}\right] - N_w C_d \tag{9}$$

where Q_g and Q_w are annual production of gas and water (m^3), respectively; P_g is wellhead gas price ($/$m^3$); C_w is cost of treatment and disposal of produced water ($/$m^3$); T is the producing lifetime of the target area (year); C_d is the cost of well construction ($/well); C_m is the cost of operating expense per well per year ($); R_t is tax rate on the produced gas; i_0 is the annual discount rate (%); and N is the total number of wells drilled.

2.4. Numerical reservoir simulator

Production profiles for each scenario of well placement are generated by conducting reservoir simulation using CMG's GEM simulator. The GEM is a three-dimensional compositional simulator that is capable of simulating the sorption, diffusion and flow phenomena of CBM transport in coal and it is widely used in CBM reservoir and production engineering studies (Karacan and Olea, 2015; Karacan et al., 2014; Salmachi and Karacan, 2017). Details of the mathematical models regarding the CBM module in GEM can be found in GEM (2015), which are therefore not repeated in this paper.

2.5. Optimization procedure

The general workflow of well spacing and placement optimization is illustrated in Fig. 4 and described briefly as follows.

1) Randomly initialize well pattern indices and spacings.
2) Calculate the location of each well using Eqs. 1 through 6.
3) Call GEM to conduct reservoir simulations and to calculate the objective function values based on the simulated production profiles.
4) Update well pattern description index and spacings with PSO.
5) Repeat Steps 2 through 4 until the preset maximum number of iterations is reached.
6) Set the optimal well placement determined from Steps 1 through 5 as the initial solution point of GPS; in this step, the initial perturbation vector **x'** = {0,0, …,0}.
7) Update well perturbation vectors **x'** using the GPS until the preset maximum number of iterations is reached.

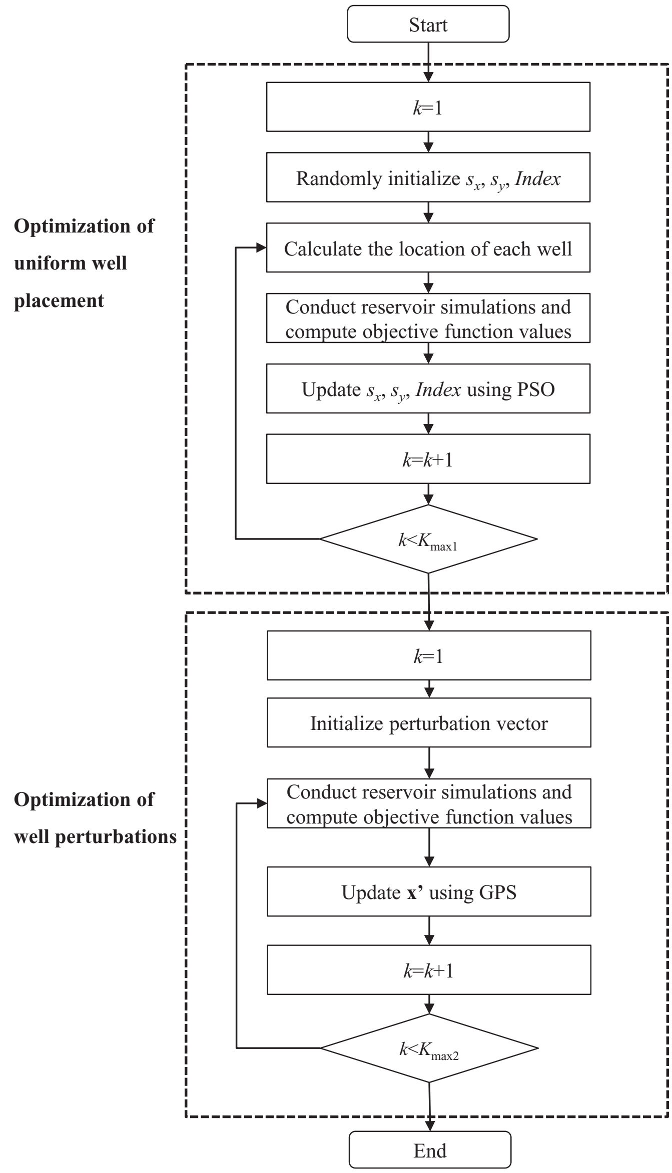

Fig. 4. Flow chart of the two-stage procedure for optimizing well placement.

3. Application of the optimization procedure for case studies

In this section, the proposed step-wise procedure is applied for optimizing well placement in two CBM reservoirs. The first case involves a synthetic model that is representative of the geological conditions of an anthracite CBM reservoir in the Qinshui basin, China. The second case is a real high-volatile bituminous coalbed in the Illinois basin that has been built and calibrated by Karacan et al. (2014).

3.1. Case 1: well placement in a synthetic model

3.1.1. Model description

In this case, a synthetic model was constructed to represent the typical geological features of low permeability and high gas content reservoirs in anthracite coals of the Qinshui basin, China (Liu et al., 2013; Lv et al., 2012). The model consists of 80 × 80 × 1 grid blocks in the X-, Y- and Z-direction, respectively. Each grid block has a dimension of 20 m × 20 m in the lateral plane. Heterogeneities in formation thickness, permeability and gas content are included in this model, which are shown in Fig. 5. Permeability evolution due to pressure drawdown and matrix shrinkage (see e.g., Chen et al., 2013; Li and

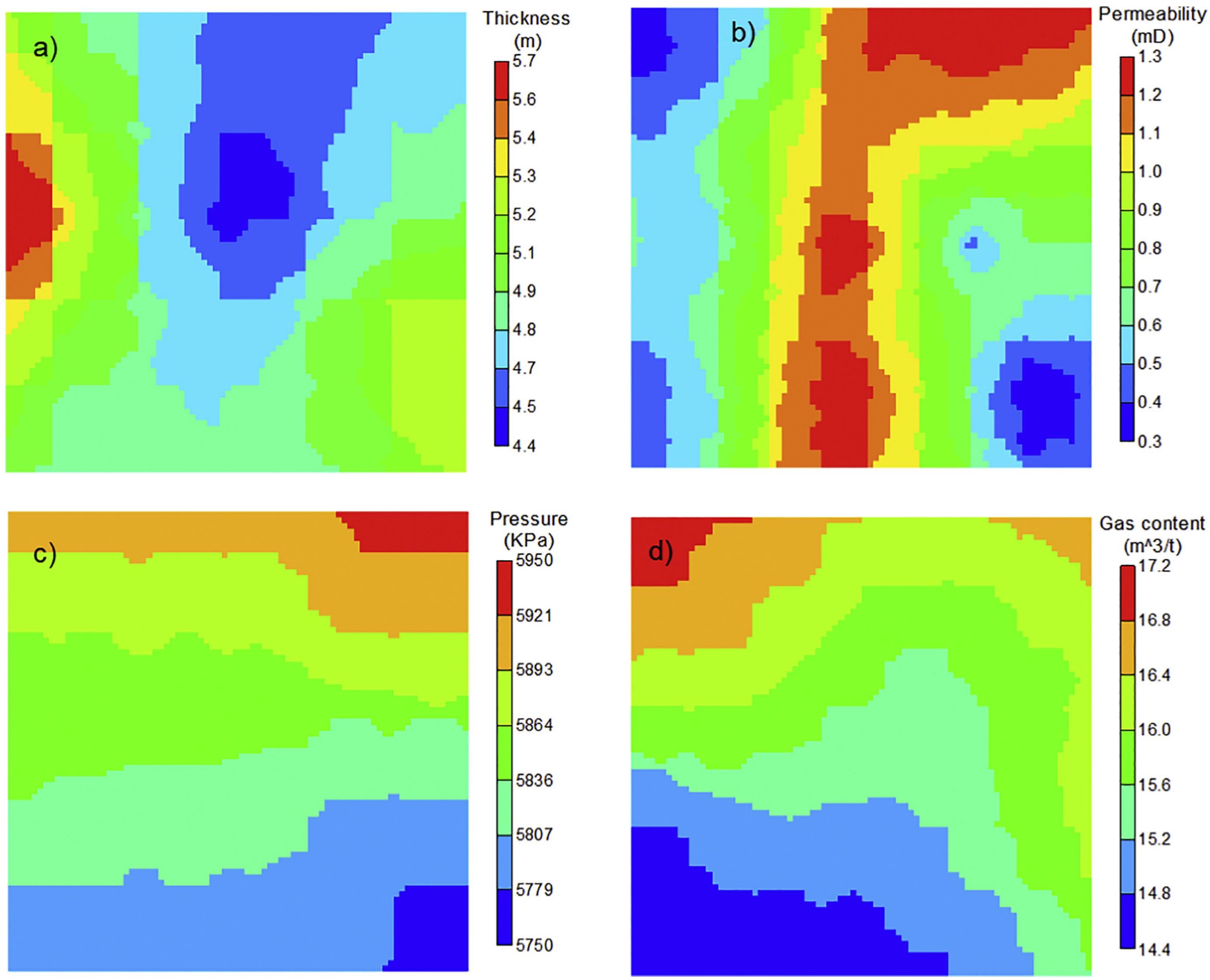

Fig. 5. Spatial distribution of (a) formation thickness, (b) permeability and (c) cleat pressure and d) gas content of the synthetic model.

Table 1
Reservoir properties for the reservoir models.

Parameter	Synthetic model	Real field model
Reservoir depth (m)	576–594	157–186
Formation thickness(m)	4.41–5.65	0.69–2.13
Permeability (mD)	0.33–1.29	38–117
Porosity (−)	0.02	0.01–0.06
Pressure (KPa)	5760–5940	1505–1787
Gas content (m^3/t)	14.5–17.1	3.18–3.75
Rock compressibility (KPa^{-1})	1.5×10^{-5}	2.5×10^{-5}
Sorption strain (−)	0.02	0.012
Langmuir pressure for sorption stain curve (KPa)	4500	4500
Poison ratio (−)	0.21	0.21
Young's modulus (KPa)	1.5×10^6	2.9×10^6
Langmuir volume (m^3/t)	30	11.1–12.1
Langmuir pressure (KPa)	3000	3920
Desorption time (d)	1	20
Temperature (K)	313.15	311.6
Bulk density (kg/m^3)	1300	1400

Elsworth, 2015; Wu et al., 2010) is represented by a modified Palmer-Mansoori model (GEM, 2015; Palmer and Mansoori, 1998), with the parameters shown in Table 1. Relative permeability curves were

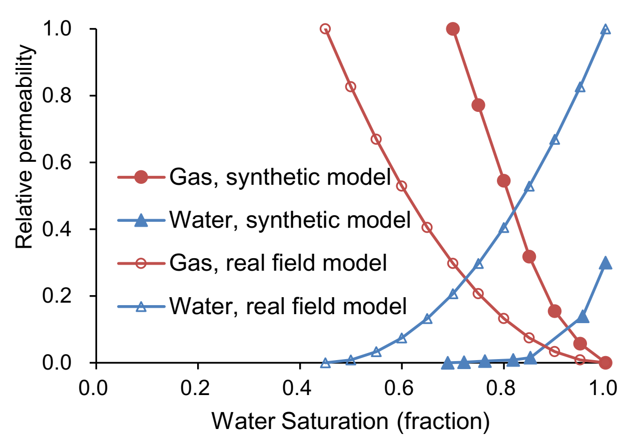

Fig. 6. Relative permeability curves used in this study.

adopted from experimental data on a Qinshui basin coal sample by Shen et al. (2011) (Fig. 6). Typically, relative permeability for coal samples in the Qinshui basin are associated with a narrow two-phase flow span and a high connate water saturation. Input reservoir properties for numerical simulations are summarized in Table 1.

Table 2
Parameterization for the PSO and GPS algorithms.

Algorithm	Parameters	Values
PSO	Swarm size	10
	Particle inertia coefficient	0.9 to 0.6
	Cognitive attraction coefficient	1.0
	Social attraction coefficient	2.0
	Max.no. of function evaluations	100
GPS	Expansion factor	5.0
	Contraction factor	0.1
	Poll method	2n positive basis
	Max. no. of function evaluations	100

Table 3
Economic parameters for computing NPV.

Parameter	Synthetic model	Real field model
Well construction (million \$/well)[a]	0.34	0.1
Gas price (\$/m^3)	0.24[b]	0.09[c]
Water disposal (\$/m^3)[d]	6.25	6.25
Well operating expense (\$/well/year)[e]	6000	6000
Annual discount rate (%)[e]	10	10
Tax rate on the produced gas (%)[e]	8	8

[a] The well construction costs include expenses for drilling, completion and surface facilities. The well drilling cost is set to be \$410/m, which is the averaged value for drillings in onshore oil/gas fields according to EIA (2016). The averaged well depths are 585 m and 170 m for the synthetic and real field models, respectively. Thus, the drilling costs are ~\$240,000 and \$70,000 for the synthetic and real field models, respectively. As implied in EIA (2016), the drilling cost takes a portion of 60–80% of the total construction costs for vertical wells. We picked a mediate value of 70% for approximating the total well construction costs based on the well drilling costs, which are ~\$3,400,000 and \$100,000 for the synthetic and real field models, respectively. The approximated well construction cost for the synthetic model agrees well with the data provided by Wu et al. (2018) for the Qinshui CBM reservoirs, although it is determined based on the EIA data for the US oil/gas fields.

[b] Adopted from Wu et al. (2018)

[c] Adopted from EIA website (https://www.eia.gov/naturalgas/data.php#prices).

[d] Adopted from EIA (2016).

[e] Adopted from Salmachi et al. (2013).

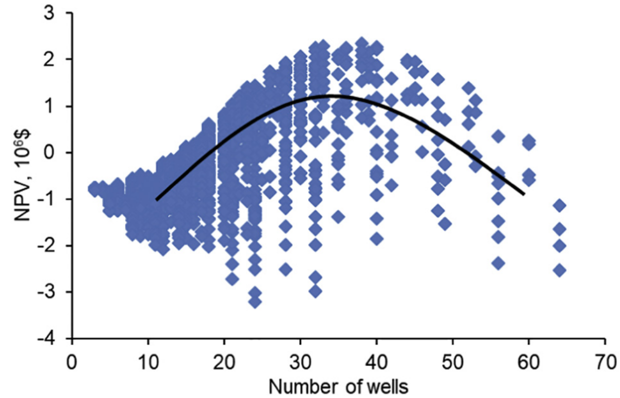

Fig. 8. Relation between the NPV and the number of wells corresponding to all possible scenarios of well pattern and spacings for the synthetic model.

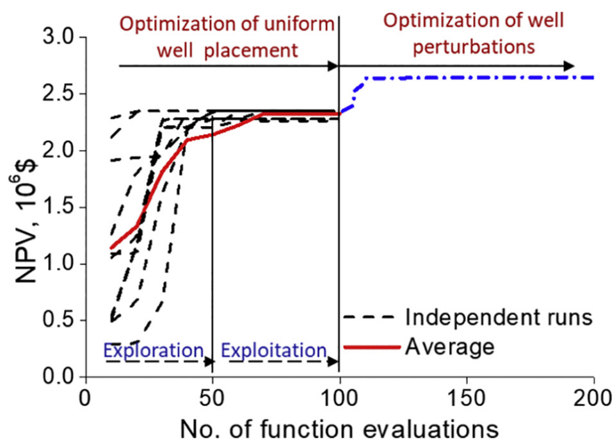

Fig. 9. NPV evolution trajectories during the first- and second-stage optimization for the synthetic model.

As a common practice, vertical wells in CBM reservoirs are usually stimulated by hydraulic fracturing to increase productivity. Ideally, using local grid refinement together with near-wellbore permeability enhancement should reflect the effect of hydraulic fracture on production more accurately (Zuber et al., 1990; Zhang and Bian, 2015). However, this approach requires more computational effort and

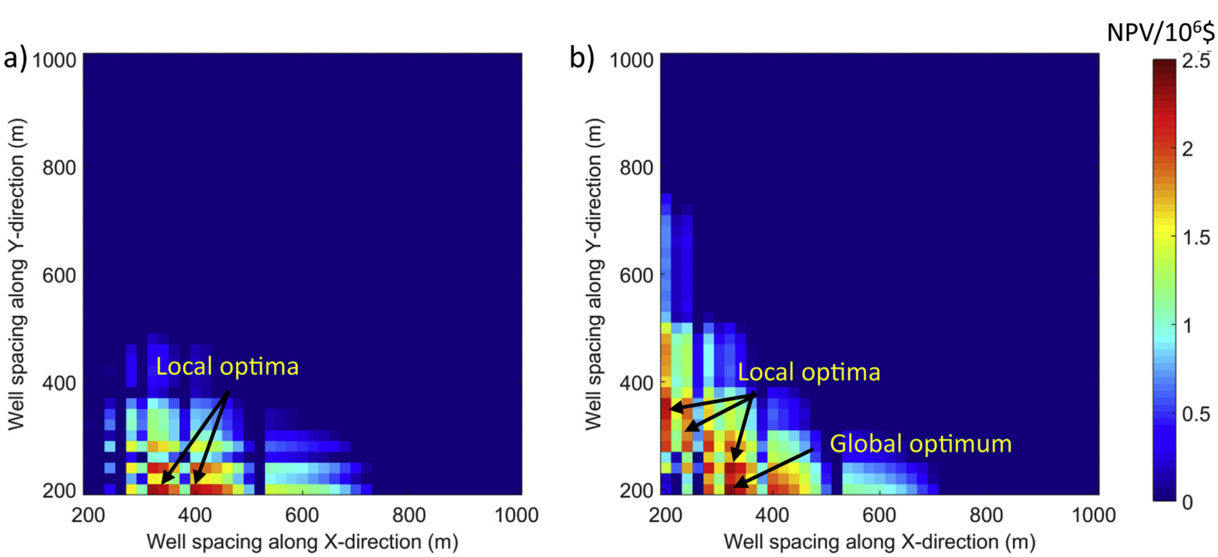

Fig. 7. The NPV surface corresponding to well spacings for (a) rectangular and (b) five-spot well pattern of the synthetic model. Note: the minimum for the NPV color bar is set to be zero for clear visualization.

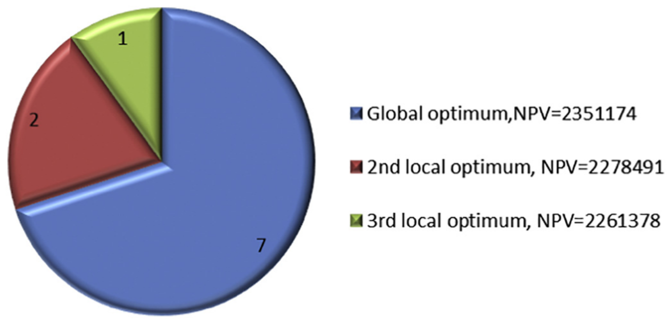

Fig. 10. Statistics of solutions resulting from 10 independent runs of the first-stage optimization for the synthetic model. The legend denotes the optimal NPVs with corresponding solutions given in Appendix A1.

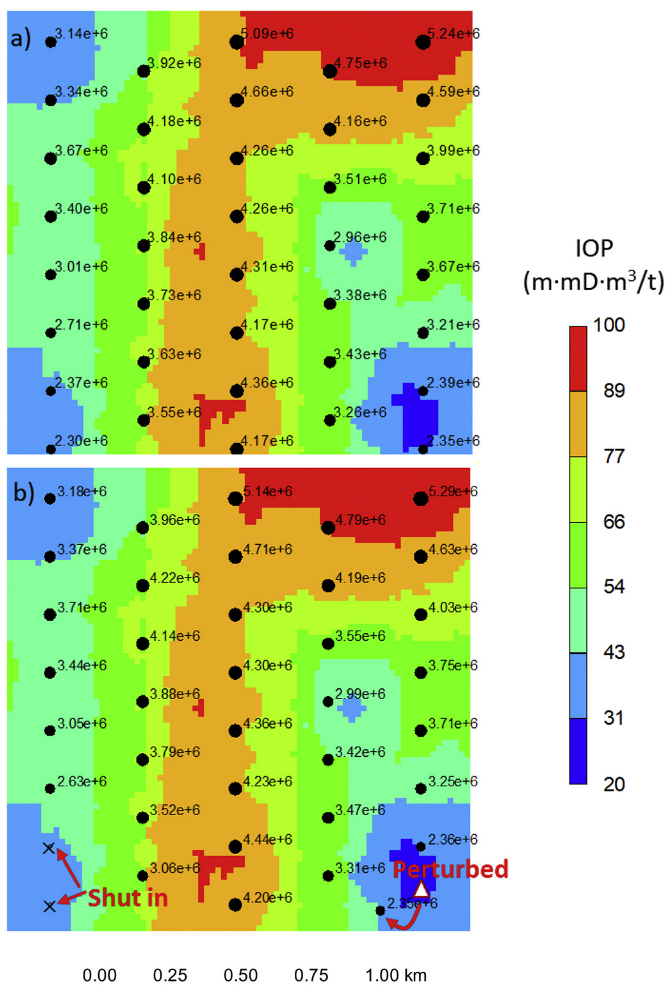

Fig. 11. Comparison of optimal well placement with a background of IOP for the synthetic model. a) uniform well placement; b) well placement with optimized perturbations. The numbers are cumulative gas productions; solid circles are active wells; triangular is the well location before perturbation; "×" denotes a well in the "shut-in" status after perturbation.

simulation time because more grid blocks are added. In this study, the effect of the hydraulic fracturing on production is considered by setting a skin factor of −4.0 on the wells (Karacan, 2013). The borehole radius is 0.076 m and all wells are operated at a constant water production rate of 10 m^3/d, which if not satisfied is turned to a constant bottom-hole pressure constraint of 0.2 MPa. The production duration is set to be 15 years, which covers the general life span of CBM wells (Feng et al., 2012; Salmachi et al., 2013; Xu et al., 2013).

The performance of an optimization algorithm is heavily dependent on its parameterization, which should be best determined through the meta-optimization (Chen et al., 2018). Since this paper is primarily concerned with the step-wise optimization framework rather than with the optimization algorithms, the meta-optimization technique is left for further investigation and is not considered here. Nonetheless, sensitivity analyses of the effect of optimization parameterizations on the algorithm performance were conducted (see Appendix A1) and the optimal parameter settings are summarized in Table 2. The maximum number of function evaluations is set to be 100 for both the PSO and GPS algorithms.

The lower boundary of both well spacings along the X- and Y-directions was set to be 200 m, with the consideration of avoiding penetration of hydraulic fractures into adjacent wells by assuming a maximum fracture half-length of 100 m. For low-permeability coal seams in Qinshui basin, optimal well spacings are generally less than 400 m × 400 m (Meng et al., 2018; Yan, 2015). However, a preliminary sensitivity analysis on this synthetic model indicates that using a loose upper boundary for well spacing tends to increase the probability of success to find the global optimum (see Appendix A2). As such, the upper boundary was expanded to 1000 m to allow the algorithm to search over a large well spacing range across the reservoir model. Economic parameters used for the computation of NPV are set according to recent published data (Table 3), with an attempt to mimic the actual cases.

3.1.2. Results

In this section, we will first report the global optimal uniform well placement determined by manually simulating all possible well pattern and spacing realizations. The proposed optimization procedure is then applied and validated by comparing the optimization with the manual simulation results.

3.1.2.1. Manual determination of the optimal uniform well placement. Under the well spacing boundary setting of 200 to 1000 m, a total of 41 × 41 × 2 = 3362 realizations of uniform well patterns are possible given a well block dimension of 20 m × 20 m. By manually conducting numerical simulations of all these possible realizations, one can obtain the gas and water rates, which can then be used together with economic parameters (Table 3) to compute the NPV surfaces (Fig. 7). As shown in Fig. 7, the NPV surfaces are extremely rough and multiple local optimal points are demonstrated especially in the lower left triangular region of the NPV surfaces. To quantitatively compare the local optima solutions, we summarized the top 45 solutions with relatively high NPVs in Appendix 3, which shows that all these solutions give well spacings in the range of 200 to 460 m. Such small well spacings are quite typical for, and commonly deployed in, the low-permeability CBM formations in the Qinshui basin (Meng et al., 2018; Yang and Ye, 2008). It also shows that the top 5 solutions are associated with close NPVs – the lowest NPV among these solutions is \$2.254 × 10^6 (rectangular pattern with well spacings of 400 m × 200 m), which is only ~4.1% less than the global optimal NPV of \$2.351 × 10^6 (five-spot pattern with well spacings of 320 m × 200 m). The presence of these multiple near-optimal solutions may increase the challenge for the algorithm to find the global optima.

Fig. 8 shows the NPVs relative to the number of wells corresponding to all possible 3362 realizations of well pattern and spacing. The figure shows that the resulting NPVs first show a general increase and then decrease with the number of wells. Such an observation agrees well with that of Liu et al. (2019), which can be interpreted as a result of the competition between incomes recovered from selling the gas and well layouts of varying well numbers. Numerous studies (e.g., Chaianansutcharit et al., 2001; Gentzis and Bolen, 2008; Liang et al., 2011; Young et al., 1992) have proven that the well interference effect tends to promote reservoir pressure drawdown and accelerate gas

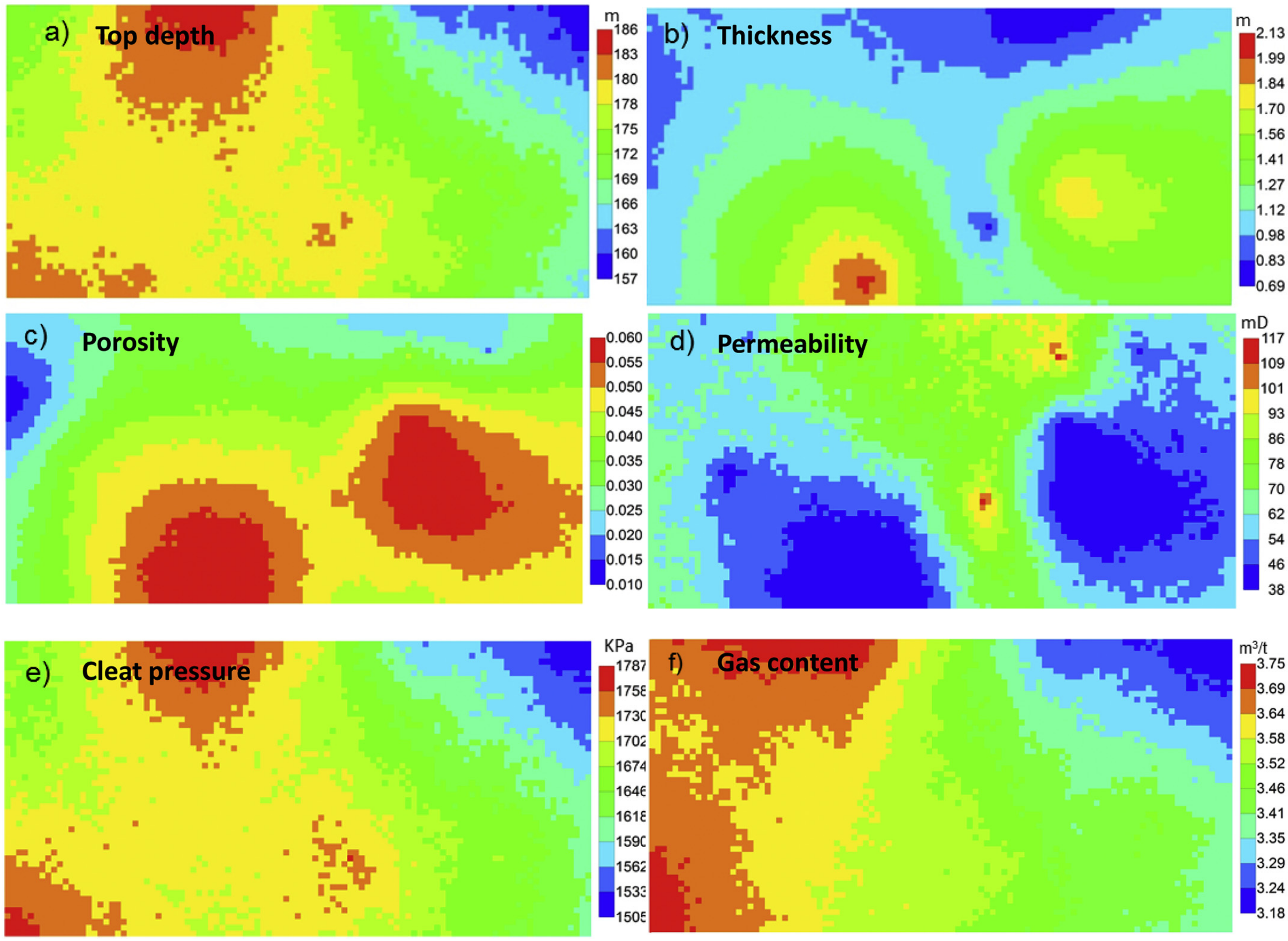

Fig. 12. Spatial distributions of reservoir properties in the real field model. (a) top depth, (b) thickness, (c) porosity, (d) permeability, (e) cleat pressure, and (f) gas content.

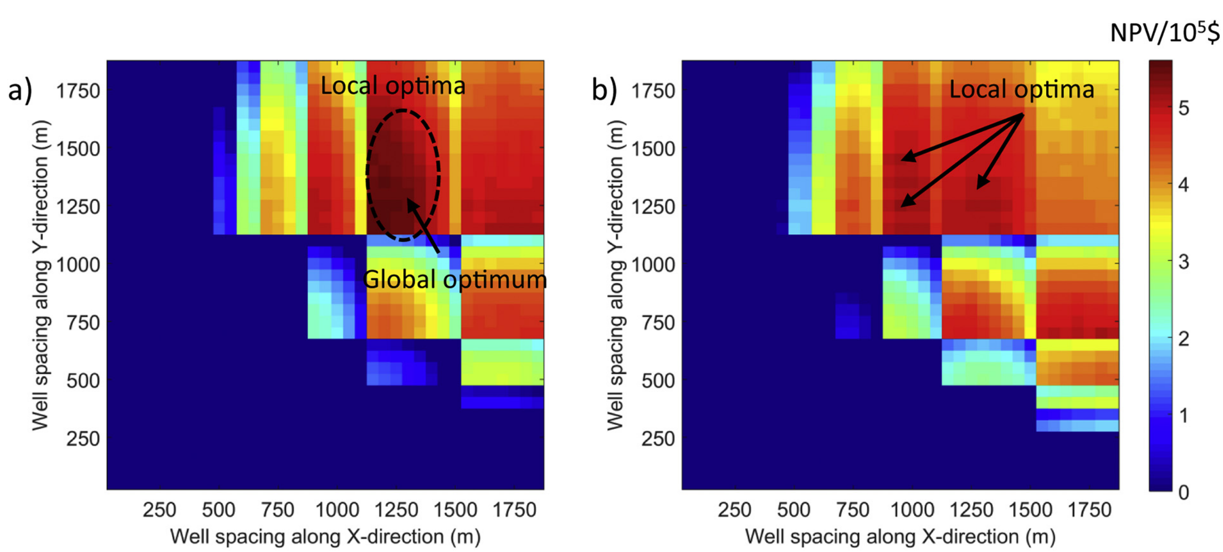

Fig. 13. The NPV surface corresponding to well spacings for (a) rectangular and (b) five-spot well pattern of the real field model. Note: the minimum for the NPV color bar is set to be zero for clear visualization.

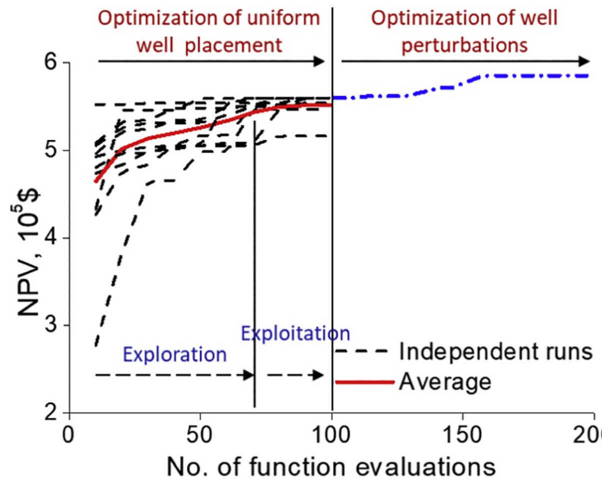

Fig. 14. NPV evolution trajectories during the first- and second-stage optimization for the real field model.

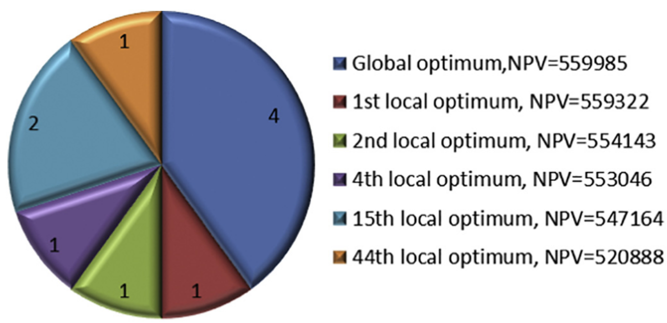

Fig. 15. Statistics of solutions resulted from 10 independent runs of the first-stage optimization for the real field model. The legend denotes the optimal NPVs with corresponding solutions given in Appendix A1.

desorption, which therefore is a predominantly favorable factor in incrementing gas production in a CBM reservoir. Drilling more wells within the reservoir tends to amplify the well interference effect, which contributes to increasing CBM production. However, drilling more wells will also increase well construction investments and operating expenses. It should be pointed out that although different realizations of well pattern and spacing may result in the same number of wells, their corresponding NPVs can vary rather significantly. For example, the lowest and highest NPVs obtained by using 32 wells are $\sim -$ \$3.00 $\times$ 10^6 and 2.254 $\times$ 10^6, respectively, which highlights the necessity of the optimization of well pattern and spacings.

3.1.2.2. Application of the optimization procedure. Since the optimal uniform well placement has been obtained by manually scanning all possible realizations, we can then apply the proposed optimization procedure and evaluate its validity by comparing the optimization with the previous results.

First, 10 independent optimization runs of uniform well pattern and spacings using the PSO were conducted, and the evolution trends of NPVs are demonstrated in Fig. 9. As shown, NPVs are non-uniform and scattered during the initial exploration stage (~50 function evaluations) of optimization, which is attributed to the stochastic nature of the initialization and velocity update schemes of the PSO algorithm. Nonetheless, all runs tend to switch from an exploration to an exploitation pattern (Kaveh, 2014) at ~50 function evaluations and then converge gradually to an optimal or near-optimal solution after a number of 100 function evaluations. Fig. 10 summarizes the optimal solutions found by 10 independent runs. As shown, 7 runs succeed in finding the global optimum with an NPV of \$2.351 $\times$ 10^6. Although the remaining 3 runs fail in reaching a global optimum, they give rather close approximations to the global optimum solution. The minimal optimized NPV among these 10 runs is \$2.261 $\times$ 10^6, which is only ~3.8% less than the global optimal NPV of \$2.351 $\times$ 10^6. The failure in reaching the global optimal solution is attributed to the presence of multiple local optimal solutions that are located around the global optimum (Fig. 7), where the PSO may be easily trapped. Nonetheless, the computational efficiency of the application of the PSO for optimizing uniform well placement is clearly demonstrated: one can recover a general high-quality solution after only 100 function evaluations using the proposed method, whereas 3362 function evaluations are needed if all possible realizations are simulated manually.

After the first-stage optimization for uniform well placement, the optimization of well perturbations can be subsequently conducted to further improve the solution and thereby, the economics. In this stage, we assume that the global optimal solution to the uniform well placement (five-spot pattern with well spacings of 320 and 200 m in the X- and Y-directions, respectively) has been successfully obtained although the first-stage optimization may result in a local optimal solution. We will discuss how a near-optimal uniform well placement solution affects the subsequent perturbation optimization results in Section 4.2. Since the GPS is deterministic in nature, the optimization results are identical provided that the starting points where optimization initiates are constant. Therefore, the performance of the GPS regarding perturbation optimization can be evaluated based on a single optimization run.

As illustrated in Fig. 9, the NPV first exhibit a substantial increase in the initial stage (10 simulation runs) and then becomes relatively stable towards the end of the perturbation optimization stage. The NPV after 100 objective function evaluations improves from \$2.351 $\times$ 10^6 to \$2.641 $\times$ 10^6, with a percentage increase of ~12.3%. Fig. 11 compares the optimal uniform and optimal perturbed well placements. It can be seen that in this particular example, the location and well status of most wells (35 out of 38) remain unchanged after well perturbation optimization. This is in accordance with previous statements in Section 2.2 and in Onwunalu and Durlofsky (2011), that the contribution of well perturbation optimization to NPV improvement is less significant than that of uniform well pattern optimization because the uniform well placement is already a near-optimal solution to the well placement optimization problem. Nonetheless, it is interesting that three wells with the least cumulative gas productions ($\leq$2.37 $\times$ 10^6 m^3) among 38 wells are perturbed after the perturbation optimization. Among the three perturbed wells, two in the lower left part of the reservoir (with a respective cumulative gas production of 2.37 $\times$ 10^6 and 2.30 $\times$ 10^6 m^3) are shut in; the remaining one (with a cumulative gas production of 2.35 $\times$ 10^6) in the lower right part of the reservoir is shifted to a grid block with higher IOP than its previous location.

3.2. Case 2: well placement in a real field model

3.2.1. Model description

The real field model used in this study is adopted from Karacan et al. (2014) that consists of a total of 101 $\times$ 51 $\times$ 1 grid blocks, each with a lateral dimension of 50 m $\times$ 50 m. This model is for the Seelyville coal located in the Indiana section of the Illinois Basin, which was constructed by means of geostatistical modeling integrated with history matching (Karacan, 2013; Karacan et al., 2014). The target formation is a high-volatile bituminous coal, which is characterized with low formation thickness, high permeability and low gas content. Such a geological condition is significantly different from that of the synthetic model, which could possibly be associated with a distinguished optimal well placement solution.

Input reservoir properties for the numerical simulations are summarized in Table 1. Fig. 12 depicts distributions of burial depth, thickness, cleat porosity, permeability, pressure and gas content of the model. As shown, significant heterogeneities are demonstrated concerning formation thickness, porosity and permeability. Reservoir

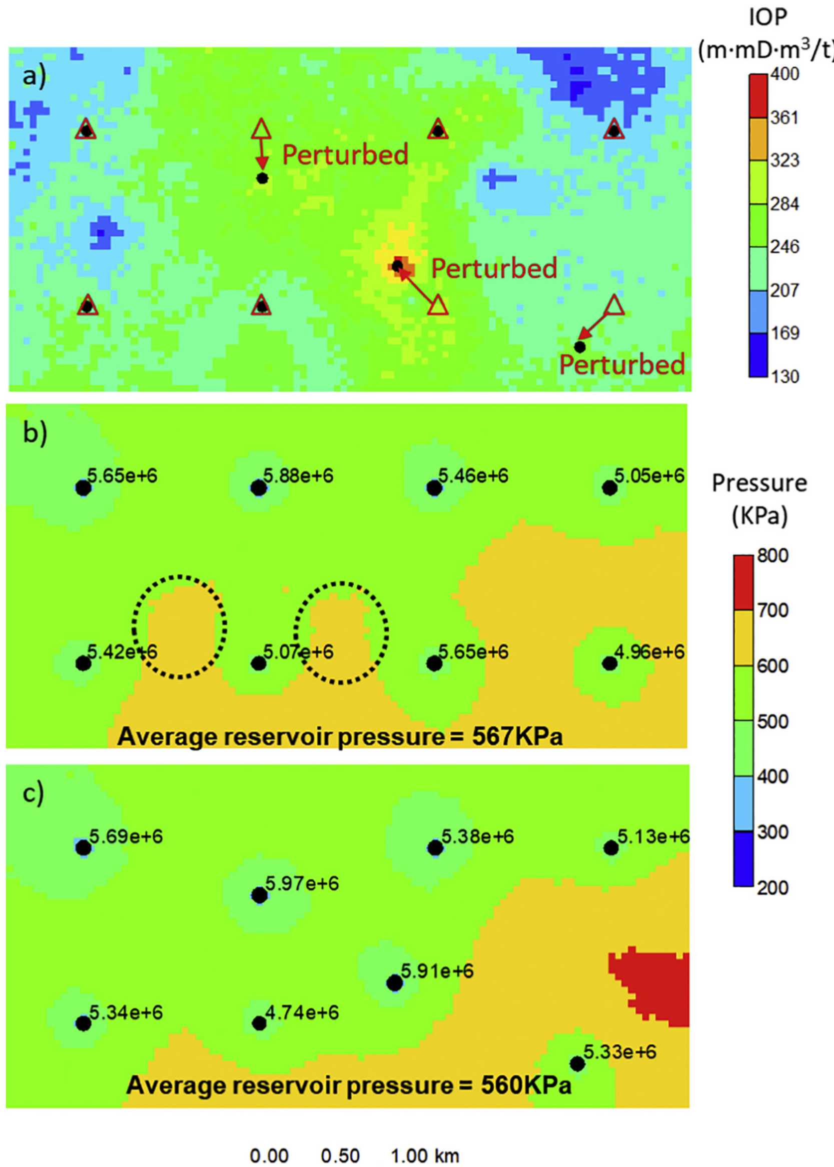

Fig. 16. Optimized well placement for the real field model. (a) comparison of the uniform optimal well pattern and well placement after perturbation optimization with a background showing the IOP.; (b) and (c) show the reservoir pressure distributions after 15 years' production using the optimal uniform and the optimal perturbed well placements, respectively. Note: Triangular and solid circles represent wells before and after perturbation optimization, respectively; the arrows illustrate how wells are perturbed; numbers are cumulative gas productions after 15 years' production.

pressure and gas content vary in a relatively narrow range, suggesting a less notable heterogeneity. Relative permeability curves were taken as "averaged" curves used in Karacan et al. (2014), which are depicted in Fig. 6. Well settings and the optimization algorithm parameterization are identical to those used in the synthetic model. The economical parameters are shown in Table 3. It is noted that the average permeability for the real field model is significantly higher than the synthetic model, and therefore the upper boundary for well spacing should be accordingly enlarged (Zulkarnain, 2005). Previous studies (Young et al., 1992 ; Zuber et al., 1990) suggest that optimal well spacings for bituminous CBM reservoirs are generally less than 640 acres (~1600 m × 1600 m). For this real field model, the upper boundary constraint for well spacing is set to be 2000 m to ensure an extensive search range.

3.2.2. Results

Similar to the procedure in Section 3.1.2, we first report the uniform well placement determined by manually scanning all possible realizations and then apply and validate the proposed optimization procedure for this real field model case.

3.2.2.1. Manual determination of the optimal uniform well placement. The optimal uniform well placement was determined by manually simulating all possible well pattern and spacing realizations (in a similar manner as in the synthetic case) to be a rectangular pattern with well spacings of 1300 and 1300 m along X- and Y-directions, respectively. The optimal well spacing is relatively large compared to that in the synthetic model (320 m × 200 m), which may be partly attributed to the relatively high permeabilities of the Seelyville coal seams. Generally, lower-permeability CBM reservoirs require smaller well spacings in order to accelerate the depressurization of the reservoir (Zulkarnain, 2005). Meanwhile, this real field model has a thin coal seam and less gas content compared with the synthetic model, where profitability can be significantly reduced using smaller well spacings (more wells) because the in situ CBM reserves is limited and drilling more wells may not contribute to significant improvement in gas

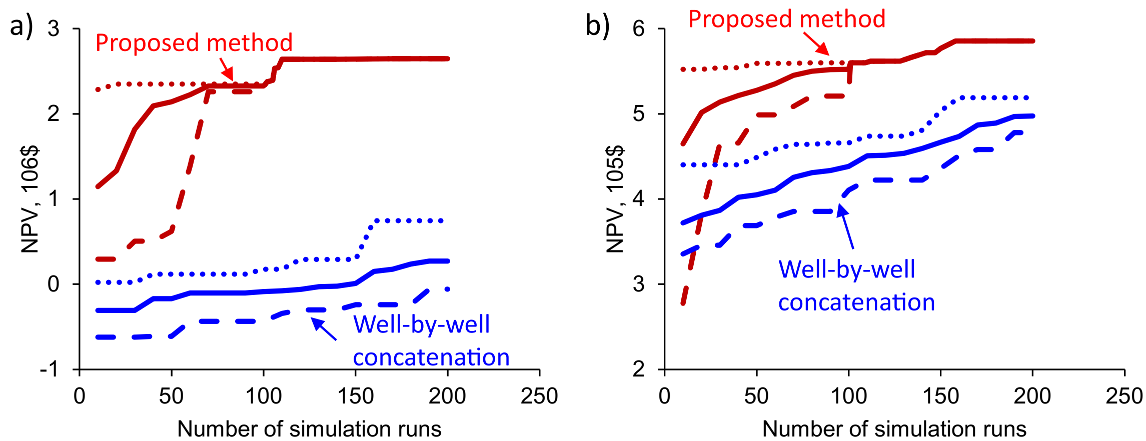

Fig. 17. Comparison of the NPV evolution trajectories using well-by-well concatenation and the proposed two-stage optimization methods for the (a) synthetic and (b) real field model.

productions. Our results are in accordance with previous studies (Young et al., 1992; Zuber et al., 1990; Zulkarnain, 2005) that conclude an increase in permeability and/or gas content tends to enlarge the optimal well spacings.

Fig. 13 shows that the NPV surface for all possible scenarios of well spacings and patterns. It is demonstrated that multiple local optimal solutions are grouped around the global optimum especially for the rectangular well pattern. Appendix A3 summarizes the top 45 most productive solutions for uniform well placement solutions with relatively high NPVs. It can be seen all these solutions give a rectangular pattern with well spacings in the range of (1300–1800) m and (1300–1500) m along the X- and Y-directions, respectively. The global optimal solution has well spacings of 1300 and 1300 m along the X- and Y-directions, respectively, with an NPV of \$5.60 $\times$ 10^5. The presence of such large number of local optimal solutions may magnify the difficulty for the PSO to find the global optima, which will be addressed in the following section.

3.2.2.2. Application of the proposed optimization procedure. For the uniform well placement optimization stage, 10 independent runs were conducted for this real field model and the trajectories of NPVs are illustrated in Fig. 14. As shown, the NPVs evolve in a similar manner to those of the synthetic model – all runs tend to be in an effective exploration state where significant improvements in NPVs are demonstrated and then converge gradually to the global optima or near-optimal solutions. Compared with the synthetic model, more simulation runs are needed in the exploration stage, which may be due to the presence of more local optima in the real field model (Fig. 7). Fig. 15 summarizes the final optimized NPVs at the end of uniform well placement optimization (100 function evaluations) for 10 independent runs. It can be seen that there are chances that the PSO algorithm gets stuck in a local optimum – only 4 runs succeed in finding the global optimal NPV of \$5.600 $\times$ 10^5 while the remaining 6 runs result in optimized NPVs less than but close to \$5.600 $\times$ 10^5.

For the well perturbation optimization stage, we again assume that the global optimal solution (rectangular pattern with well spacings of 1300 and 1300 m along the X- and Y-directions, respectively) has been successfully obtained during the uniform well placement optimization stage. The effect of a near-optimal uniform well placement solution on the subsequent perturbation optimization results will be presented in Section 4. It can be seen from Fig. 14 that the NPV climbs gradually from \$5.600 $\times$ 10^5 to \$5.856 $\times$ 10^5 within 100 functional evaluations during the perturbation optimization stage. An improvement of ~ \$2.56 $\times$ 10^4 (4.6%) in NPV can be obtained after perturbation optimization, compared with that of the optimal uniform well pattern. Such improvement in NPV is rather limited, which is may be attributed to the subtle difference in reservoir depressurizations that is to be discussed as follows.

Fig. 16a compares the well placement optimized in the first and second optimization stages. As shown, 3 among 8 wells were placed in their respective grid block with higher IOP after perturbation optimization, while the remaining 5 wells remain in their initial position. All wells remain active after well perturbation optimization, which suggest that none of these wells is redundant. Figs. 16b and c show that cumulative gas productions are increased for the three perturbed wells compared with the uniform well placement. It is also shown that well placement following optimal perturbations results in further pressure drawdown especially in the inter-well regions (which is marked with circles in Fig. 16b) compared with using the optimal uniform well placement. As stated previously, increased depressurization is favorable to gas production in CBM reservoirs, which therefore contributes to the improvement in NPVs. However, it is noted that very minor difference is demonstrated regarding the average reservoir pressures after 15 years' production using the uniform and perturbed well placements (Figs. 16b and c). Such minor difference is attributed to the relatively high permeability of the formation, which is favorable for accelerating and thus reduces the effect of well placement on pressure drawdown propagation.

4. Discussion

4.1. Comparison with the well-by-well concatenation optimization

4.1.1. Well-by-well concatenation optimization

The well-by-well concatenation optimization method is widely used for optimizing well placement in hydrocarbon reservoirs (Chen et al., 2018; Feng et al., 2012; Salmachi et al., 2013). In this method, the location of each well is represented with its special coordinates. For a multiple well placement optimization problem, the special coordinates of wells are simultaneously tuned such that an objective function (e.g., NPV) can be optimized. Unlike the proposed step-wise optimization procedure, the number of wells subject to placement optimization must be presumed before optimization initiates. For example, if we consider the placement optimization of a number of N_t wells in a single coal seam, there should be a number of 2 $\times$ N_t variables representing the X- and Y-coordinates of these wells that are to be optimized. One should note that the optimal well placement solutions are significantly affected by the presumed number of wells, which however can hardly be determined accurately prior to the well placement optimization.

In this study, the number of wells was set to be the same as that in the best uniform well pattern solution for each model case. Two sorts of infeasible solutions may be produced in well-by-well concatenation

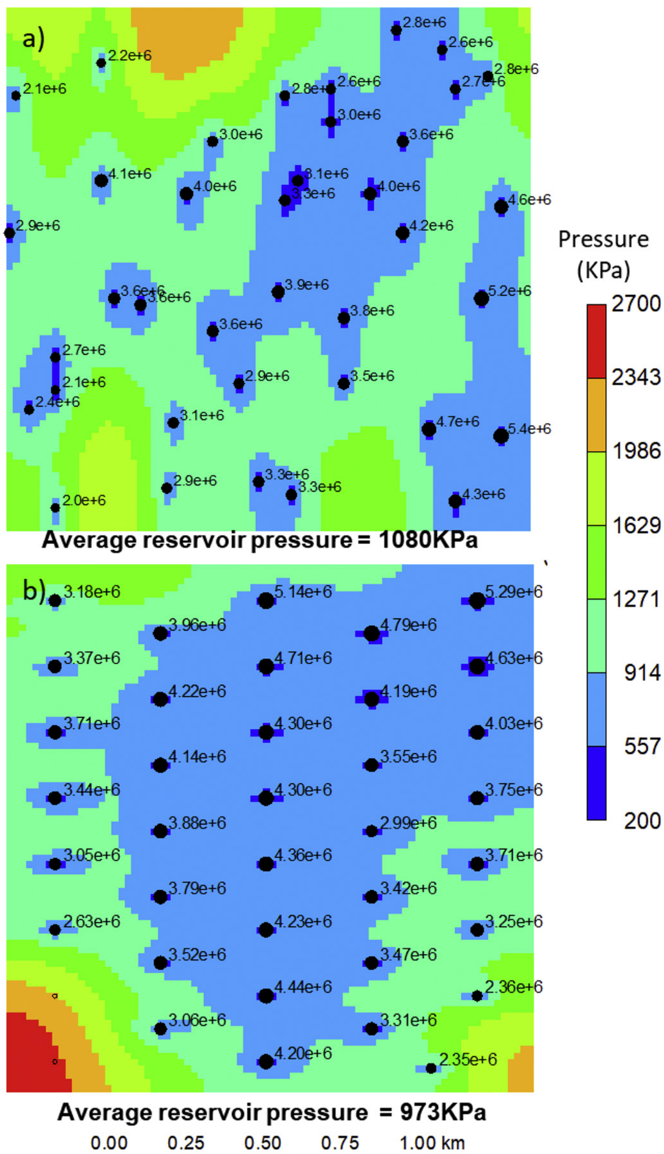

Fig. 18. Comparison of the well placement in the synthetic model obtained by the a) well-by-well concatenation and b) proposed two-stage optimization methods, with the background showing the reservoir pressure distribution after 15 years' production. Note: for the well-by-well concatenation optimization method, the solution with a highest NPV among 10 runs is shown in this figure; Numbers are cumulative gas productions after 15 years' production.

optimizations. The first infeasible solution is for a well that exists in or out of the reservoir boundary, which is handled with a "bounce back" strategy (Feng et al., 2012). The second infeasible solution is that which results in the overlapping of wells, i.e., two or more wells are placed in the same grid block. In this case, only one well at the grid block where overlapping occurs was set to be active and all other overlapping wells were assigned as "shut-in." The well construction and operating expenses of shut-in wells are eliminated from the calculation of NPV.

4.1.2. Comparison of the optimal NPV

Fig. 17 illustrates the evolution trends of NPVs for 10 runs of well-by-well concatenation optimizations as a comparison to the proposed procedure for both the synthetic and real field models. It clearly shows that none of the 10 runs results in an NPV higher than the two-stage procedure for either model. The best NPVs among 10 runs of well-by-well concatenation optimizations are \$7.471 $\times$ 10^5 and \$5.189 $\times$ 10^5 for the synthetic and real field model, respectively. Compared with the best runs of the two-stage optimization procedure, the percentage reductions in NPV using the well-by-well optimization method are ~71.8% and ~ 11.4% for the synthetic and real field models, respectively. It is also noted that severe deviations exist in NPVs between different well-by-well concatenation optimization runs. For example, the worst solution for the synthetic model has an optimized NPV of \$-5.771 $\times$ 10^4, corresponding to a relative deviation of ~100% with reference to the best solution with an NPV of \$7.471 $\times$ 10^5. This indicates the strong intrinsic instability in the well-by-well concatenation optimization procedure, and therefore multiple optimization runs should be conducted to guarantee a near-optimum solution when using the well-by-well optimization procedure. Fig. 17 also demonstrates that the convergence speed of the well-by-well optimization procedure is obviously slower than the two-stage procedure and therefore more simulation runs are needed to reach a high-quality solution in a single optimization run. Because field-scale reservoir simulations are usually time-consuming and computationally expensive, the proposed two-stage optimization procedure obviously outperforms the well-by-well concatenation optimization in terms of computational efficiency.

4.1.3. Comparison of the optimal well placement

Fig. 18 compares the optimal well locations for the synthetic model obtained by the well-by-well concatenation and the proposed optimization procedures. It is shown that the spatial distribution of well locations is highly irregular as obtained by the well-by-well concatenation optimization - some wells are grouped close to one another that results in sufficient local reservoir depressurization while some areas not controlled by wells are poorly drained. As a comparison, the proposed optimization procedure results in more evenly distributed well placement and more effective reservoir depressurization. The average reservoir pressures after a production duration of 15 years are 1080 and 973 KPa using the optimal well placements determined by the well-by-well concatenation and the proposed procedures, respectively. Such noticeable difference in reservoir depressurization is responsible for the significant difference in NPVs optimized by either procedure.

Fig. 19 depicts the optimal well placement for the real field model using the well-by-well concatenation method. Comparison between Fig. 19 and Fig. 16c shows that the reservoir pressure drawdown using the well placement optimized by the proposed procedure (560 KPa) is slightly higher than that by the well-by-well concatenation method (584 KPa). Such difference in the reservoir depressurization is less noticeable than that for the synthetic model, which is again attributed to the relatively high permeability of the Seelyville coal seams.

4.2. Effects of the first stage solution on the second stage results

As mentioned in Section 3, the PSO may be potentially trapped in local optima during the first stage of optimization (of uniform well placement) due to the extremely rough and coarse solution surface. In this section, we will discuss how a local optimal solution obtained in the first stage affects the optimization results in the second stage. For the synthetic model, the top three local optimal solutions, as summarized in Appendix A3, are used for sensitivity analysis with the consideration that all optimization runs give a solution with NPVs higher than \$2.261 $\times$ 10^6 (which is ranked as the 3rd local optimal solution, see Fig. 10). For the real field model, the 15th, 30th and 45th local optimal solutions are analyzed.

As shown in Fig. 20a, for the synthetic model, the final optimal NPVs after 100 objective function evaluations during the perturbation stage are generally dependent on the initialization - a higher NPV obtained during the first optimization stage results in a higher NPV during the second stage. As stated in Section 3.1, only three wells (out of a total of 38 wells) are perturbed during the well perturbation optimization stage. Under the constraint of a *narrow* well spacing defined by the uniform well placement optimization, the contribution of well perturbation to NPV improvements is significantly compressed, which

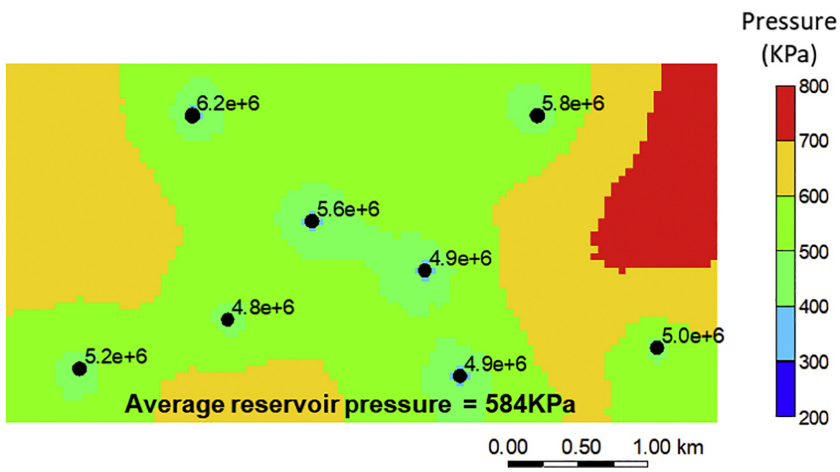

Fig. 19. Optimal well placement obtained by the well-by-well concatenation optimization method for the real field model with a background showing the reservoir pressure distribution and numbers representing cumulative gas productions after 15 years' production.

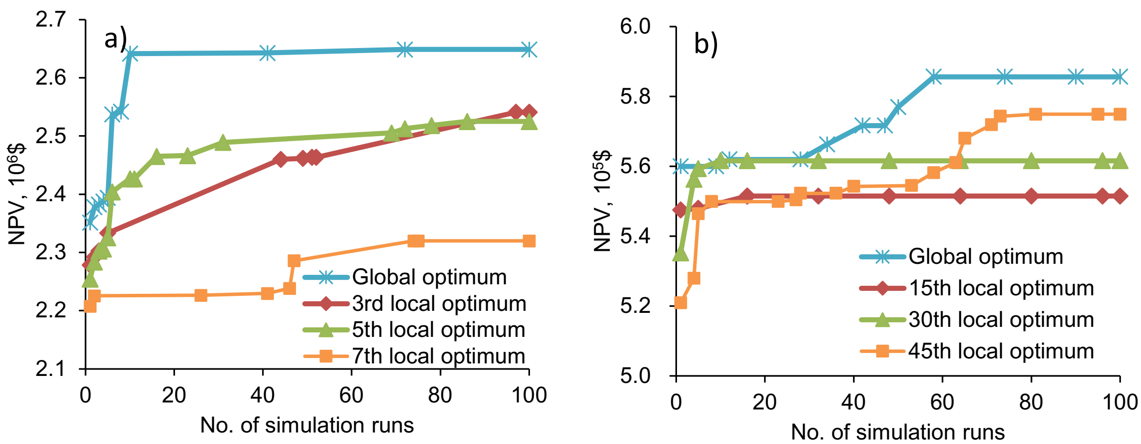

Fig. 20. Sensitivity analysis of the effect of the first-stage optimization solution on the NPV evolution during the second-stage (well perturbation) optimization processes for the (a) synthetic and (b) real field models.

therefore signifies the effect of the uniform well placement solution. As such, several optimization runs may be needed in practice to screen the PSO solutions in order to guarantee a high quality well perturbation solution. Nonetheless, it is noted that the PSO is highly efficient in delivering the global optimum (Figs. 9 and 10) and therefore multiple optimization runs should take limited additional computational costs.

Fig. 20b shows that the solution of the first optimization stage affects the second optimization stage in a quite different manner for the real field model, compared with that for the synthetic model. For the real field model, the difference between the highest (\$5.856 $\times$ 10^5) and lowest (\$5.515 $\times$ 10^5) optimal NPVs after well perturbations using different initializations is only \$3.41 $\times$ 10^4, which suggest a very minor effect of the first-stage solution on the second-stage optimization results. It is also shown in Fig. 20b that a better uniform well placement solution does not guarantee a higher NPV after well perturbation optimization. For example, i) the solution with the 15th local optimum determined in the first optimization stage result in a lowest NPV after well perturbation optimization and ii) the resulting NPV using the 30th local optimum is lower than the 45th. One possible explanation for this observation is that the optimal or near-optimal uniform well spacings are relatively large for the real field model, and therefore wells can be perturbed within a more expansive space than that in the synthetic model. This results in more flexible well perturbations and tends to weaken the predominant effect of the initial uniform well placement. Besides, as mentioned in Section 3.2, this real field model has relatively high reservoir permeability, and similar average reservoir pressure drawdown may be attained even for different well placement patterns provided the number of wells is identical. Such findings suggest that local optimal solutions in the first optimization stage do not significantly affect the final NPVs after the optimization of perturbation.

5. Conclusions

This paper proposes a general framework to optimize well placement for large-scale field development of CBM through integration of reservoir simulations, optimization algorithms and economics. The optimization framework consists of two stages – viz. optimization of uniform well placement and then optimization of perturbations in well locations. The framework was applied to obtain the optimal well placement in both a synthetic and then a real field CBM reservoir, both of which were demonstrated to outperform the well-by-well concatenation optimization method in terms of computational efficiency and NPV. Sensitivity analysis suggests that for an optimal uniform well placement pattern with narrow well spacings in the synthetic model with low permeability, the contribution of well perturbation to the NPV increment is heavily dependent on the uniform well placement solution. For an optimal uniform well placement pattern with relatively large well spacings in the real field model with high permeability, the initial uniform well placement has a very minor effect on the subsequent well perturbation solutions.

Declaration of Competing Interest

The authors declare that they have no known competing financial interests or personal relationships that could have appeared to influence the work reported in this paper.

Acknowledgment

This research was conducted under the financial support of PCSIRT (IRT1294), the National Natural Science Foundation of China (Grant Nos. U1762213, U1810105, 51904319), the Fundamental Research Funds for the Central Universities (Grant No. 18CX02105A) and China Postdoctoral Science Foundation (Grant No. 2018M642727).

Disclaimer

This paper has been peer reviewed and approved for publication consistent with U.S. Geological Survey Fundamental Science Practices (http://pubs.usgs.gov/circ/1367/). Any use of trade, firm, or product names is for descriptive purposes only and does not imply endorsement by the U.S. Government.

Appendix A. Supplementary data

Supplementary data to this article can be found online at https://doi.org/10.1016/j.coal.2020.103479.

References

ARI, 2002. Powder River basin coalbed methane development and produced water management study. In: Technical report DOE/NETL-2003/1184.

Audet, C., Dennis Jr., J.E., 2002. Analysis of generalized pattern searches. SIAM J. Optim. 13 (3), 889–903.

Badri, M., Dare, D., Rodda, J., Thiesfield, G., Blauch, M., 2000. Keys to the successful application of hydraulic fracturing in an emerging coalbed methane prospect-an example from the peat coals of Australia. SPE 64493.

Bangerth, W., Klie, H., Wheeler, M.F., Stoffa, P.L., Sen, M.K., 2006. On optimization algorithms for the reservoir oil well placement problem. Comput. Geosci. 10, 303–319.

Bank G.C, Kuuskraa, V.A., 2006. The economics of Powder River Basin coalbed methane development. In: Technical report.

Bumb, A.C., McKee, C.R., 1984. Use of a computer model to design optimal well for dewatering coal seams for methane production. In: Paper SPE 12859.

Cai, Y., Liu, D., Yao, Y., Li, J., Qiu, Y., 2011. Geological controls on prediction of coalbed methane of no. 3 coal seam in southern Qinshui Basin, North China. Int. J. Coal Geol. 88 (2–3), 101–112.

Chaianansutcharit, T., Che, H.-Y., Teufel, L.W., 2001. Impacts of permeability anisotropy and pressure interference on coalbed methane (CBM) production. In: Paper SPE 71069.

Chen, Z., Liu, J., Elsworth, D., Pan, Z., Wang, S., 2013. Roles of coal heterogeneity on evolution of coal permeability under unconstrained boundary conditions. J. Nat. Gas Sci. Eng. 15 (6), 38–52.

Chen, H., Feng, Q., Zhang, X., Wang, S., Ma, Z., Zhou, W., Liu, C., 2018. A meta-optimized hybrid global and local algorithm for well placement optimization. Comput. Chem. Eng. 117, 209–220.

Chen, H., Feng, Q., Zhang, X., Wang, S., Zhou, W., Liu, F., 2019. Well placement optimization with cat swarm optimization algorithm under oilfield development constraints. J. Energy Res.Technol. 141, 012902.

Clarkson, C.R., McGovern, J.M., 2005. Optimization of CBM reservoir exploration and development strategies through integration of simulation and economics. SPE Reserv. Eval. Eng. 8 (6), 502–519.

Ding, S., Jiang, H., Li, J., Tang, G., 2014. Optimization of well placement by combination of a modified particle swarm optimization algorithm and quality map method. Comput. Geosci. 18 (5), 747–762.

Ding, S., Lu, R., Xi, Y., Wang, S., Wu, Y., 2019. Well placement optimization using direct mapping of productivity potential and threshold value of productivity potential management strategy. Comput. Chem. Eng. 121, 327–337.

EIA, 2016. Trends in U.S. oil and natural gas upstream costs. In: Technical report.

Feng, Q., Zhang, J., Zhang, X., Hu, A., 2012. Optimizing well placement in a coalbed methane reservoir using the particle swarm optimization algorithm. Int. J. Coal Geol. 104, 34–45.

Forouzanfar, F., Reynolds, A.C., 2014. Joint optimization of number of wells, well locations and controls using a gradient-based algorithm. Chem. Eng. Res. Des. 92 (7), 1315–1328.

GEM, 2015. User guide: compositional & unconventional reservoir simulator. Calgary, Canada.

Gentzis, T., Bolen, D., 2008. The use of numerical simulation in predicting coalbed methane producibility from the Gates coals, Alberta Inner Foothills, Canada: Comparison with Mannville coal CBM production in the Alberta Syncline. Int. J. Coal Geol. 74 (3), 215–236.

Humphries, T.D., Haynes, R.D., 2015. Joint optimization of well placement and control for nonconventional well types. J. Pet. Sci. Eng. 126, 242–253.

Humphries, T.D., Haynes, R.D., James, L.A., 2014. Simultaneous and sequential approaches to joint optimization of well placement and control. Comput. Geosci. 18 (3–4), 433–448.

Isebor, O.J., Durlofsky, L.J., Ciaurri, D.E., 2014. A derivative-free methodology with local and global search for the constrained joint optimization of well locations and controls. Comput. Geosci. 18 (3–4), 463–482.

Jesmani, M., Bellout, M.C., Hanea, R., Foss, B., 2016. Well placement optimization subject to realistic field development constraints. Comput. Geosci. 20 (6), 1185–1209.

Karacan, C.Ö., 2013. Production history matching to determine reservoir properties of important coal groups in the Upper Pottsville Formation, Brookwood and Oak Grove fields, Black Warrior Basin, Alabama. J. Nat. Gas Sci. Eng. 10 (1), 51–67.

Karacan, C.Ö., Olea, R.A., 2015. Stochastic reservoir simulation for the modeling of uncertainty in coal seam degasification. Fuel 148, 87–97.

Karacan, C.Ö., Ruiz, F.A., Cotè, M., Phipps, S., 2011. Coal mine methane: a review of capture and utilization practices with benefits to mining safety and to greenhouse gas reduction. Int. J. Coal Geol. 86, 121–156.

Karacan, C.Ö., Drobniak, A., Mastalerz, M., 2014. Coal bed reservoir simulation with geostatistical property realizations for simultaneous multi-well production history matching: a case study from Illinois Basin, Indiana, USA. Int. J. Coal Geol. 131, 71–89.

Kaveh, A., 2014. Advances in Metaheuristic Algorithms for Optimal Design of Structures. Springer.

Keim, S.A., Luxbacher, K.D., Karmis, M., 2011. A numerical study on optimization of multilateral horizontal wellbore patterns for coalbed methane production in Southern Shanxi Province, China. Int. J. Coal Geol. 86, 306–317.

Kennedy, J., Eberhardt, R.C., 1995. Particle swarm optimization. In: Proceedings of the IEEE International Joint Conference on Neural Networks, pp. 1942–1947.

Li, X., Elsworth, D., 2015. Geomechanics of CO_2 enhanced shale gas recovery. J. Nat. Gas Sci. Eng. 26, 1607–1619.

Liang, B., Chen, T., Sun, W., 2011. Well interference on well pattern arrangement of complicatedly geologic CBM reservoirs. In: The 11th National Conference on Fluid mechanics in Porous Media, China, 301–307, (in Chinese with English abstract).

Liu, H., Sang, S., Formolo, M., Li, M., Liu, S., Xu, H., An, S., Li, J., Wang, X., 2013. Production characteristics and drainage optimization of coalbed methane wells: a case study from low-permeability anthracite hosted reservoirs in southern Qinshui Basin, China. Energy Sust. Develop. 17 (5), 412–423.

Liu, J., Liu, R., Luo, D., Zhai, Y., 2019. CBM economic well density optimization model and application. Natural Gas and Oil 37 (1), 115–121 (in Chinese with English abstract).

Luo, D.K., Dai, Y.J., Xia, L.Y., 2011. Economic evaluation based policy analysis for coalbed methane industry in China. Energy 36, 360–368.

Lv, Y., Tang, D., Xu, H., Luo, H., 2012. Production characteristics and the key factors in high-rank coalbed methane fields: a case study on the Fanzhuang Block, southern Qinshui Basin, China. Int. J. Coal Geol. 96–97, 93–108.

Meng, Z., Zhang, K., Yang, J., Lei, J., Wang, Y., 2018. Analysis of coal reservoir characteristics in the Qinnan-East block and its spacing optimization of CBM development well networks. J. China Coal Soc. 43 (9), 2525–2533 (in Chinese with English abstract).

Moore, T.A., 2012. Coalbed methane: a review. Int. J. Coal Geol. 101, 36–81.

Nakajima, L., Schiozer, D.J., 2003. Horizontal well placement optimization using quality map definition. In: Paper PETSOC-2003-053.

Onwunalu, J., 2010. Optimization of field development using particle swarm optimization and new well pattern descriptions. PhD thesis. Stanford University.

Onwunalu, J.E., Durlofsky, L.J., 2010. Application of a particle swarm optimization algorithm for determining optimum well location and type. Comput. Geosci. 14 (1), 183–198.

Onwunalu, J.E., Durlofsky, L.J., 2011. A new well-pattern-optimization procedure for large-scale field development. SPE J. 16 (3), 594–607.

Ozkan, E., Clarkson, C.R., 2012. Editorial for the special issue: Unconventional natural gas. J. Nat. Gas Sci. Eng 8, 1.

Palmer, I., 2010. Coalbed methane completions: a world view. Int. J. Coal Geol. 82 (3–4), 184–195.

Palmer, I., Mansoori, J., 1998. How permeability depends on stress and pore pressure in coalbeds: a new model. SPEREE 1 (6), 539–544.

Pashin, J.C., 2010. Variable gas saturation in coalbed methane reservoirs of the Black Warrior Basin: implications for exploration and production. Int. J. Coal Geol. 82 (3), 135–146.

Ren, J., Zhang, L., Ren, S., Lin, J., Meng, S., Ren, G., Gentzis, T., 2014. Multi-branched horizontal wells for coalbed methane production: field performance and well structure analysis. Int. J. Coal Geol. 131, 52–64.

Ross, H.E., Hagin, P., Zoback, M.D., 2009. CO_2 storage and enhanced coalbed methane recovery: reservoir characterization and fluid flow simulations of the big George coal, Powder River Basin, Wyoming, USA. Int. J. Greenhouse Gas Control 3 (6), 773–786.

Salmachi, A., Karacan, C.Ö., 2017. Cross-formational flow of water into coalbed methane reservoirs: controls on relative permeability curve shape and production profile. Environ. Earth Sci. 76 (5), 200.

Salmachi, A., Sayyafzadeh, M., Haghighi, M., 2013. Infill well placement optimization in coal bed methane reservoirs using genetic algorithm. Fuel 111, 248–258.

Salmachi, A., Bonyadi, M.R., Sayyafzadeh, M., Haghighi, M., 2014. Identification of potential locations for well placement in developed coalbed methane reservoirs. Int. J. Coal Geol. 131, 250–262.

Shen, J., Qin, Y., Wang, G.X., Fu, X., Wei, C., Lei, B., 2011. Relative permeabilities of gas and water for different rank coals. Int. J. Coal Geol. 86 (2–3), 266–275.
Tang S., Li Z., 2013. Coalbed methane developing and well spacing method for high-water content coal reservoir of head plate. Chinese patent no. CN102926732A.
Torczon, V., 1997. On the convergence of pattern search algorithms. SIAM J. Optim. 7 (1), 1–25.
Wang, X., Haynes, R.D., Feng, Q., 2016. A multilevel coordinate search algorithm for well placement, control and joint optimization. Comput. Chem. Eng. 95, 75–96.
Wang, X., Haynes, R.D., He, Y., Feng, Q., 2019. Well control optimization using derivative-free algorithms and a multiscale approach. Comput. Chem. Eng. 123, 12–33.
Wicks, D.E., Schwerer, F.C., Militzer, M.R., Zuber, M.D., 1986. Effective production strategies for coalbed methane in the Warrior Basin. SPE 15234.
Wu, Y., Liu, J., Elsworth, D., Miao, X., Mao, X., 2010. Development of anisotropic permeability during coalbed methane production. J. Nat. Gas Sci. Eng. 2 (4), 197–210.
Wu, Y., Pan, Z., Zhang, D., Lu, Z., Connell, L.D., 2018. Evaluation of gas production from multiple coal seams: a simulation study and economics. Int. J. Min. Sci. Technol. 28, 359–371. https://doi.org/10.1016/j.ijmst.2018.03.008.
Xu, B., Li, X., Haghighi, M., Ren, W., Du, X., Chen, D., Zhai, Y., 2013. Optimization of hydraulically fractured well configuration in anisotropic coal-bed methane reservoirs. Fuel 107, 859–865.
Yan, Y., 2015. The Study on Numerical Simulation and Development Scheme of Coalbed Gas in Qin South Block. Master thesis. Northeast Petroleum University.
Yang, X., Ye, J., 2008. Well pattern optimization design for CBM development. China Coalbed Methane 5 (1), 13–17 (in Chinese with English abstract).
Yao, Y., Liu, D., Qiu, Y., 2013. Variable gas content, saturation and accumulation characteristics of Weibei coalbed methane pilot-production field in Southeast Ordos Basin, China. AAPG Bull. 97 (8), 1371–1393.
Young, G.B.C., McElhiney, J.E., Paul, G.W., McBane, R.A., 1992. A parametric analysis of Fruitland coalbed methane producibility. In: Paper SPE 24903.
Zhang, J., Bian, X., 2015. Numerical simulation of hydraulic fracturing coalbed methane reservoir with independent fracture grid. Fuel 143, 543–546.
Zhang, K., Zhang, W., Zhang, L., Yao, J., Chen, Y., Lu, R., 2014. A study on the construction and optimization of triangular adaptive well pattern. Comput. Geosci. 18 (2), 139–156.
Zhang, Y., Lu, R., Forouzanfar, F., Reynolds, A.C., 2017. Well placement and control optimization for WAG/SAG processes using ensemble-based method. Comput. Chem. Eng. 101, 193–209.
Zhou, F., Hou, W., Allinson, G., Wu, J., Wang, J., Cinar, Y., 2013. A feasibility study of ECBM recovery and CO_2 storage for a producing CBM field in southeast Qinshui Basin, China. Int. J. Greenhouse Gas Control 19, 26–40.
Zuber, M.D., Kuuskraa, V.A., Sawyer, W.K., 1990. Optimizing Well Spacing and Hydraulic-Fracture Design for Economic Recovery of Coalbed Methane. SPE Formation Evaluation, pp. 98–102 March.
Zulkarnain, I., 2005. Simulation study of the effect of well spacing, effect of permeability anisotropy, and effect of Palmer and Mansoori model on coalbed methane production. MS Thesis. A&M University, Texas.